Results and Conclusions

The impact deviation resulting from roll rate variation and constant α has been computed for an example re-entry vehicle with the following physical characteristics: $\beta = 2000$ lb/ft^2, $W = 131$ lb, $I_r = 0.34$ slug ft^2, $A = 0.92$ ft^2, and $C_{L\alpha} = 0.034$/deg. The re-entry velocity and flight-path angle were 22,690 fps and $-20°$, respectively. Roll rate variations from 1 cps down to 0.5 cps and up to 1.5, 2, 3, and ∞ cps were considered. These variations were assumed to be the result of $|\dot{P}|$ between 0.4 cps^2 and 50 cps^2. The $\dot{P}$ was initiated at an altitude of 35,000 ft and remained constant until P had varied the prescribed amount. The magnitude of the maximum impact error possible per degree of trim was computed using Eq. (46) combined with Eqs. (42) and (44), and is presented in Fig. 6. Also, the asymptotic solution corresponding to infinite $|\dot{P}|$ was computed from Eq. (51) and included in Fig. 6.

The deviation of the impact point from the zero-lift impact point which occurs as a result of lift and roll rate variation has been obtained from various six-degree-of-freedom trajectory simulations and is included in Fig. 6. The results derived from the simple model developed herein compare typically to within 5% of the results obtained from the trajectory simulations, with none of the differences exceeding 13%.

References

[1] Martin, J. M., *Atmospheric Reentry*, Prentice-Hall, N.J., 1966, pp. 78–80.

[2] Fuess, B. F., "Impact Dispersion Due to Mass and Aerodynamic Asymmetrics," *Journal of Spacecraft and Rockets*, Vol. 4, No. 10, Nov. 1967, pp. 1402–1403.

[3] Jahnke, E. and Emde, F., *Tables of Functions*, Dover Publications, New York, 1945, pp. 34–37.

[4] Chapman, D. R., "An Approximate Analytical Method for Studying Entry into Planetary Atmospheres," TN 4276, May 1968, NACA.

[5] Allen, H. J. and Eggers, A. J., Jr., "A Study of the Motion and Aerodynamic Heating of Ballistic Missiles Entering into Earth's Atmosphere at High Supersonic Speeds," TR 1381, 1958, NACA.

MAY 1971 J. SPACECRAFT VOL. 8, NO. 5

Missile Aerodynamic Predictions to 180°

MILLARD L. HOWARD* AND EUGENE N. BROOKS JR.†
Naval Ship Research and Development Center, Washington, D.C.

AND

BERNARD F. SAFFELL JR.‡
Idaho Nuclear Corporation, Idaho Falls, Idaho

A method for predicting the static, longitudinal aerodynamic characteristics of typical missile configurations at zero roll angle (i.e., in a plus configuration) has been developed and programed for use on the IBM 7090 digital computer. It can be applied throughout the subsonic, transonic, and supersonic speed regimes to slender bodies of revolution or to nose-cylinder body combinations with low-aspect-ratio lifting surfaces. The aerodynamic characteristics can be computed for missile configurations operating at angles of attack up to 180°. The effects of control surface deflections for all modes of aerodynamic control are taken into account. The method is based on linear, nonlinear-cross-flow, and slender-body theories with empirical modifications to provide the high angle-of-attack capability. Comparisons of the theory with experimental data are presented to demonstrate the accuracy of the method.

Nomenclature§

AR = exposed aspect ratio
b = semispan of an aerodynamic surface including r, ft
C_D = total drag coefficient; components of C_D are indicated by subscripts b, base; c, cross flow; f, friction; i, induced; 0, total zero-lift; p, pressure; v, wave
C_f, C_{f_c} = incompressible and compressible skin-friction coefficients
$C_{D_{fp}}$ = drag of a flat plate normal to the flow
C_L = total lift coefficient
$C_{L\alpha}$ = lift curve slope, rad^{-1}
C_m = total longitudinal pitching moment coefficient
C_r, C_t = root-chord and tip-chord of an aerodynamic surface, ft
d = body diameter at any station, ft; d_b, body base; d_N, nose-body juncture
f = spanwise location of the vortex which emanates from the forward surface, ft
h_A = height of the trailing vortex above the body center line at the aft surface center of pressure, ft
i = downwash interference constant
$(k_2 - k_1)$ = apparent mass factor
K, K' = linear lift interference factors due to α and δ
l = length, ft; l_B = body length; l_{REF} = arbitrary reference length, usually the maximum body diameter
l_T, l_W = lengths from nose tip to the intersections of the tail and wing leading edges, respectively, with the body, ft
M = freestream Mach number
m = cotangent of the leading edge sweep angle
r = radius of the body at any station, ft
Re = Reynolds number

Presented as Paper 70-981 at the AIAA Guidance, Control and Flight Mechanics Conference, Santa Barbara, Calif., August 17–19, 1970; submitted August 28, 1970; revision received January 11, 1971.

* Aerospace Engineer. Member AIAA.
† Aerospace Engineer. Associate Member AIAA.
‡ Mechanical Engineer.

§ The control surface is defined as the tail regardless of the mode of control; the fixed surface is defined as the wing (see Fig. 1).

S = area, ft²; S_B = body base area; S_F = exposed planform area of one pair of forward lifting surfaces; S_N body cross-sectional area at the nose-body junction; S_P = planform area of the body; S_S = surface area of the body

S_T,S_W = exposed planform areas of one pair of tail surfaces and one pair of wings, respectively

S_T',S_W' = S_T,S_W values obtained by extending the leading and trailing edges to the center line of the body, ft²

V_B = volume of the body, ft³

X = distance from nose, ft; X_{CG} = center of gravity; X_{CP} = center of pressure location; X_P = centroid of the body planform area

α = missile angle of attack, deg

β = compressibility factor $(M^2 - 1)^{1/2}$

δ = control surface deflection, deg

ΔC_D = component of the induced drag coefficient

ΔC_{D_0} = increment of wave drag for the transonic speed regime

η = ratio of the C_D of a circular cylinder of finite length to that of a cylinder of infinite length

θ_N = conical nose semivertex angle, deg

λ = lifting surface taper ratio, C_t/C_r

Λ = leading edge sweep angle, deg

$\Lambda_{c/4}$ = sweep angle of the quarter chord line, deg

Subscripts

A = aft lifting surface, alone

B,BT,BW = body alone, body in the presence of the tail, and body in the presence of the wing

F,FB = forward surface alone and in the presence of the body

N = nose

T,TB = tail alone and in the presence of the body

TV,WV = nonlinear components for tail and wing

W,WB = wing alone and in the presence of the body

α,δ = due to α or δ

Introduction

INCREASING maneuverability requirements of missiles indicated a need for predicting the aerodynamic characteristics, including lift, drag, and pitching moment, of missile configurations to angles of attack (α's) of 90° and higher. Existing methods for computing these aerodynamic characteristics were applicable only to small α's. To fulfill the high-α requirements, a method for determining the aerodynamic characteristics of low-aspect-ratio configurations at zero roll angle operating at α's up to 180° has been developed. It is applicable throughout the subsonic, transonic, and supersonic speed regimes up to $\beta AR \cong 10$, and accounts for control surface deflections.

The method is composed of well-known linear, cross-flow, and slender-body theories modified to provide the required high-α capability. These theories can be applied to slender bodies of revolution or nose-cylinder bodies with canard, wing, or tail controls (Fig. 1).

Lift Characteristics

The total lift on the missile is the sum of the body lift, the lift due to the aerodynamic surfaces, and the interference lift between the forward and aft surfaces. The lift on the body and aerodynamic surfaces is composed of two components—linear lift including the effects of the body-lifting surface interaction and nonlinear cross-flow lift. In general, the cross-flow lift component is caused by flow separation which occurs at angles of attack.[1]

Body lift is predicted by the method of Allen,[2,3] which includes the linear or potential flow component and two nonlinear components—the viscous cross-flow force and the viscous axial force. Allen's expression is

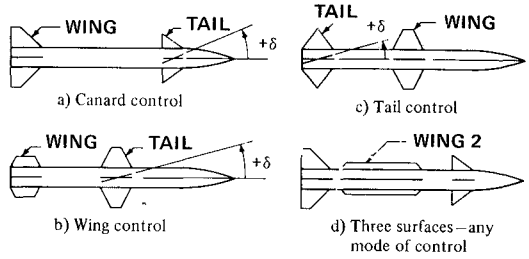

Fig. 1 Typical missile configurations.

$$C_{L_B} = (k_2 - k_1)(S_B/S_{\text{REF}}) \sin 2\alpha \cos\alpha/2 + \eta C_{d_c}(S_P/S_{\text{REF}}) \sin^2\alpha \cos\alpha - C_{D_{0_B}} \cos^2\alpha \sin\alpha \quad (1)$$

where the first term is the linear contribution and the other terms are the nonlinear contributions. The apparent mass factor $(k_2 - k_1)$, the drag ratio η, and the cross-flow drag coefficient C_{d_c} can be obtained from Allen. Comparisons of theory with experimental drag for numerous bodies of revolution over wide ranges of M and α are presented by Allen and Perkins.[3]

When the diameter of the missile body is of the same order of magnitude as the span of the lifting surfaces, the effects of body-wing and body-tail interactions are significant. Hence, the linear lift of the aerodynamic surface is composed of the lift on the surface in the presence of the body, and the added lift on the body due to the presence of a surface. Most low-aspect-ratio missile configurations exhibit a nonlinear dependence of lift on α, especially at the higher angles. One primary cause of this is the cross-flow lift component which is due to lateral flow separation and the formation of free vortices on the upper surface. This nonlinear dependence is analyzed by Pitts et al.,[1] and Flax and Lawrence[4] and summarized by Eaton.[5]

The expression for the total wing lift based on an arbitrary reference area is

$$C_{L_W} = C_{L_{WB-\alpha}} + C_{L_{BW-\alpha}} + C_{L_{WV}} \quad (2)$$

In order to provide high-α capability, it is necessary to modify both the linear and nonlinear theories. The lift on the wing in the presence of the body, as presented by Pitts et al.,[1] is a linear function of α. Since the lift force does not vary linearly at high α's, it is modified such that the linear lift becomes a function of $\sin\alpha$. This component of the linear lift is modified further to satisfy the end condition of zero lift at $\alpha = 90°$, resulting in the expression for the linear wing lift in the presence of a body

$$C_{L_{WB-\alpha}} = K_{BW} C_{L_{\alpha_W}} (S_W/S_{\text{REF}}) \sin\alpha \cos\alpha \quad (3)$$

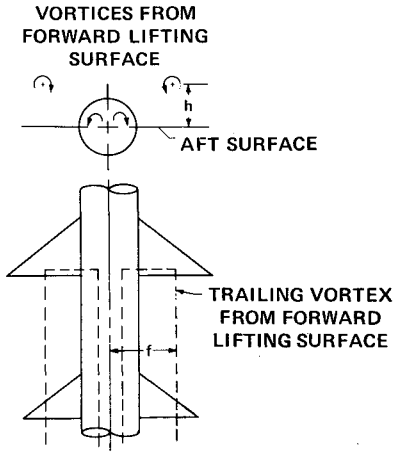

Fig. 2 Vortex model used to determine the lift loss due to downwash.

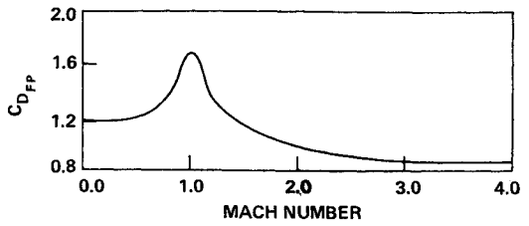

Fig. 3 Drag coefficient for a flat plate normal to the flow.

(For small α the modified theory should be very close to the method of Pitts et al., since $\sin\alpha \approx \alpha$, and $\cos\alpha \approx 1$.) Similarly, the additional lift on the body due to the presence of the wing is

$$C_{L_{BW-\alpha}} = K_{BW} C_{L\alpha_W} (S_W/S_{REF}) \sin\alpha \cos\alpha \qquad (4)$$

The parameters, K_{WB} and K_{BW} are given by Pitts et al.,[1] in graphic form and equation form. Franz[7] gives $C_{L\alpha_W}/AR$ curves, and $C_{L\alpha_W}$ is obtained by multiplying Franz's curves by AR if $AR < 1$. When $AR > 1$, the equation

$$C_{L\alpha_W} = [1/AR^{(AR-1)/AR}](C_{L\alpha_W}/AR)AR \qquad (5)$$

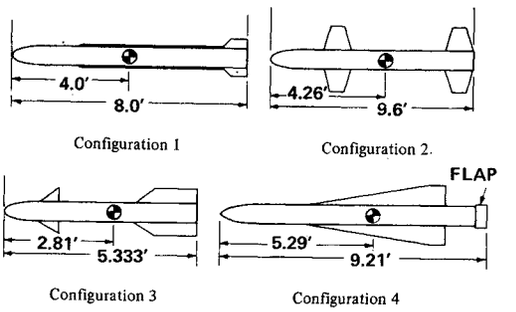

Fig. 4 Configurations used to compare theory with experiment.

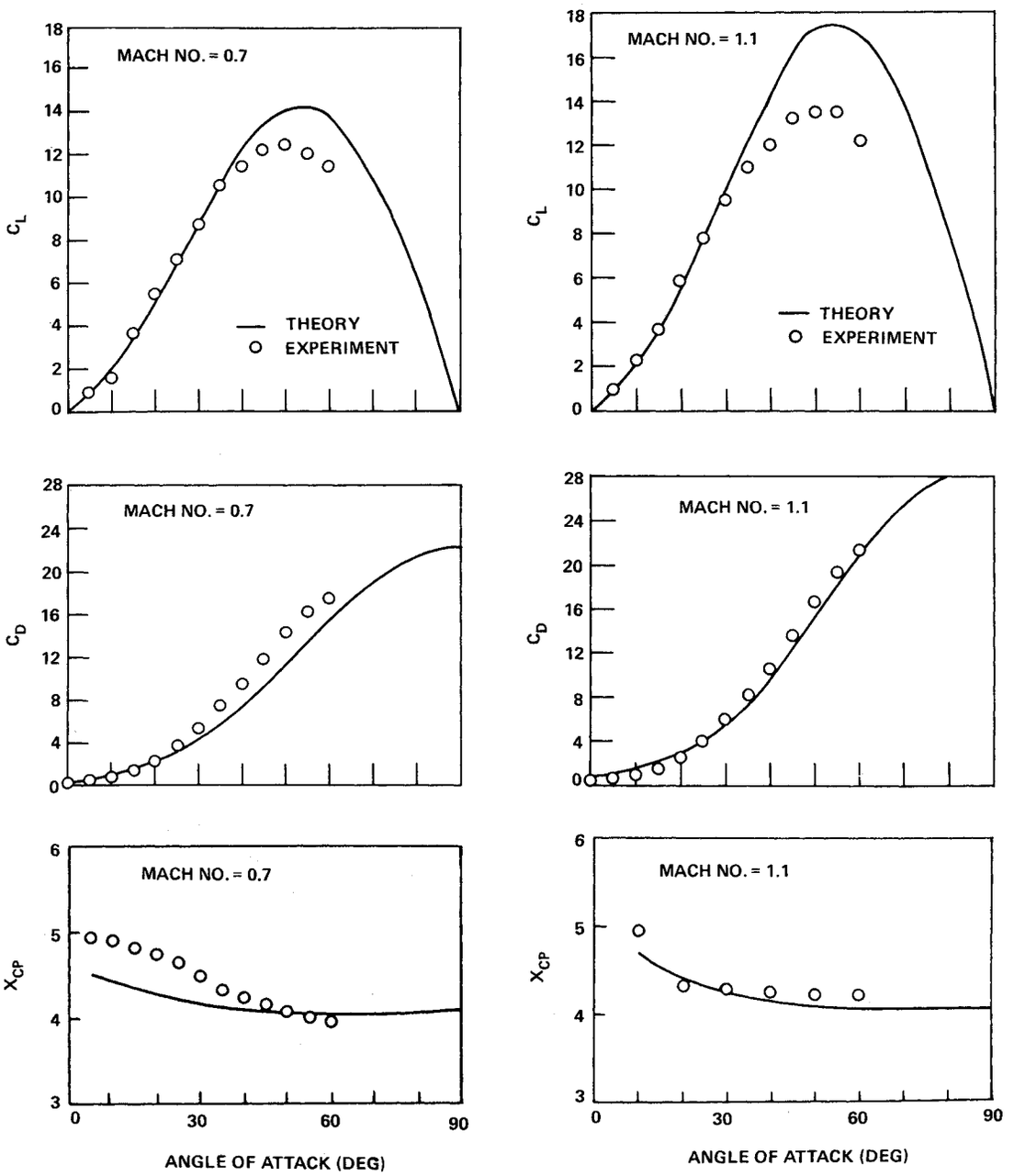

Fig. 5 Comparison of experimental data with theoretical results for configuration 1.

is used. The first term of Eq. (5) is an empirical modification of the lift curve slope for lifting surfaces with $AR > 1$.

The nonlinear wing lift from Eaton[5] is modified to satisfy the end condition at $\alpha = 90°$. The expression becomes

$$C_{L_{WV}} = C_{d_c} \sin^2\alpha(S_W/S_{REF}) \cos\alpha \quad (6)$$

where C_{d_c} is obtained from Gersten.[6] The cross-flow drag coefficient is not appreciably affected by M[5,6]; hence, C_{d_c} is presented independent of M. The total tail lift is basically the same as the wing lift except for the lift due to δ. The tail lift is expressed as

$$C_{L_T} = C_{L_{TB-\alpha}} + C_{L_{BT-\alpha}} + C_{L_{TB-\delta}} + C_{L_{BT-\delta}} + C_{L_{TV}} \quad (7)$$

where $C_{L_{TB-\alpha}}$ and $C_{L_{BT-\alpha}}$ are obtained by applying Eqs. (5) and (6) to the tail surface. The other three components are

$$C_{L_{TB-\delta}} = K_{TB}' C_{L\alpha_T} \sin\delta \frac{S_T}{S_{REF}} \cos(\alpha + \delta) \quad (8)$$

$$C_{L_{BT-\delta}} = K_{BT}' C_{L\alpha_T} \sin\delta \frac{S_T}{S_{REF}} \cos(\alpha + \delta) \quad (9)$$

$$C_{L_{TV}} = C_{d_c} \sin^2(\alpha + \delta) \frac{S_T}{S_{REF}} \cos(\alpha + \delta) \quad (10)$$

The parameters K_{BT}' and K_{TB}' are obtained from Pitts et al.[1] and $C_{L\alpha_T}$ and C_{d_c} are obtained as specified for the wing. Notice that the nonlinear lift is based on the local angle of attack, $(\alpha + \delta)$, of the control surface.

The lift-loss on the aft surface due to downwash from the forward surface for the entire speed range is obtained from the method presented by Pitts et al., and discussed by Gersten.[6] Since the method[1] is complex and lengthy, only the equations necessary to compute the lift-loss are presented. The nomenclature used to describe the lifting surfaces is changed from wing and tail to forward and aft surfaces. This is necessary because the control surface whether it be a wing, canard, or tail is designated the tail and because the aft surface regardless of the mode of control is the one which is affected by downwash.

The lift-loss due to downwash is

$$C_{L_i} = \frac{C_{L\alpha_F} C_{L\alpha_A} (K_{FB} \sin\alpha + K_{FB}' \sin\delta_F) i (b - r)_A SF}{2\pi (AR)_A (f - r_F) S_{REF}} \quad (11)$$

This equation is obtained from line-vortex theory assuming only one trailing vortex per forward panel exists (see Fig. 2). The lateral location f and the vertical location h of the vortex are required for use in Eq. (11) and to compute the interference factor i. The fraction of the exposed semispan is

$$\left(\frac{f - r}{b - r}\right)_F = \frac{\frac{\pi}{4} - \frac{\pi}{4}\left(\frac{r}{b}\right)_F^2 - \left(\frac{r}{b}\right)_F + \frac{[1 + (r/b)_F^2]^2}{2[1 - (r/b)_F^2]} \sin^{-1}\frac{1 - (r/b)_F^2}{1 + (r/b)_F^2}}{2[1 - (r/b)_F]} \quad (12)$$

For convenience, the right-hand side of this equation is defined as A'. Isolating f results in the expression

$$f = A'(b - r)_F + r_F \quad (13)$$

where f is the spanwise location of the vortex.

The vertical location of the vortex h is measured normal to the body axis at the center of pressure of the aft surface. The expression for h is

$$h = -(C_r - X_h)_F \sin\delta_F + [l_A + (\bar{X}_{CP})_A l_F - (C_r)_F] \sin\alpha \quad (14)$$

Note that the vertical location of the vortex is a function of both α and δ of the forward surface. The interference factor, i, is given by

$$i = \frac{2}{1 + \lambda}\left[L\left(\lambda, \frac{r}{b}, \frac{f}{b}, \frac{h}{b},\right) - L\left(\lambda, \frac{r}{b}, -\frac{f}{b}, \frac{h}{b}\right) - L\left(\lambda, \frac{f_i}{b}, \frac{h_i}{b}\right) + L\left(\lambda, \frac{r}{b}, \frac{f_i}{b}, \frac{h_i}{b}\right)\right] \quad (15)$$

where

$$L\left(\lambda, \frac{r}{b}, \frac{f}{b}, \frac{h}{b},\right) = \frac{(b - r\lambda) - f(1 - \lambda)}{2(b - r)} \times \ln\frac{h^2 + (f - b)^2}{h^2 + (f - r)^2} - \frac{1 - \lambda}{(b - r)} \times \left[(b - r) + h \tan^{-1}\frac{f - r}{h} - \mathrm{h} \tan^{-1}\frac{f - r}{h}\right] \quad (16)$$

and

$$f_i = r^2 f/(f^2 + h^2),\ h_i = r^2 h/(f^2 + h^2) \quad (17)$$

Hence, once the location of the vortex is determined and the position of the image vortices, f_i and h_i, is determined from Eq. (17), the interference factor can be computed from Eqs. (15) and (16). The lift-loss due to interference can then be calculated.

The total lift based on an arbitrary reference area is obtained by adding the components

$$C_L = C_{L_B} + C_{L_W} + C_{L_T} + C_{L_i} \quad (18)$$

Drag Characteristics

The total aerodynamic drag acting on a missile is the sum of the zero-lift drag, the induced drag due to α and/or δ, and the base-pressure drag. It is well-known that the selection of the proper technique for computing the zero-lift drag is determined by the operating speed of the missile. The methods employed to compute the zero-lift drag are those described in the USAF DATCOM[8] and will not be discussed here. The zero-lift drag calculations include base pressure drag.

Induced Drag

The induced drag due to angle of attack and/or tail surface deflection is composed of four drag increments as shown below.

$$C_{D_i} = \Delta C_{D_{B-\alpha}} + \Delta C_{D_{W-\alpha}} + \Delta C_{D_{T-\alpha}} + \Delta C_{D_{T-\delta}} \quad (19)$$

The drag increment for the body is obtained using a method presented by Allen and Perkins,[3] while the induced drag due to the wing and tail is obtained from the drag of an equivalent flat plate normal to the flow. The induced drag on a body of revolution at angle of attack can be expressed as follows:

$$\Delta C_{D_{B-\alpha}} = (k_2 - k_1) \frac{S_B}{S_{REF}} \sin^2\alpha \sin\frac{\alpha}{2} + \eta C_{d_c} \frac{S_p}{S_{REF}} \sin^3\alpha \quad (20)$$

The wing induced drag based on an arbitrary reference area is obtained from

$$\Delta C_{D_{W-\alpha}} = C_{D_{FP}}(S_W \sin\alpha)/S_{REF} \quad (21)$$

where $C_{D_{FP}}$ is the drag of a flat plate normal to the flowfield, and is determined from Fig. 3. The drag curve shown in Fig. 3 has been constructed using the three-dimensional subsonic drag coefficient for a flat plate normal to the flow[10] and the variation of the drag coefficient with Mach number for the

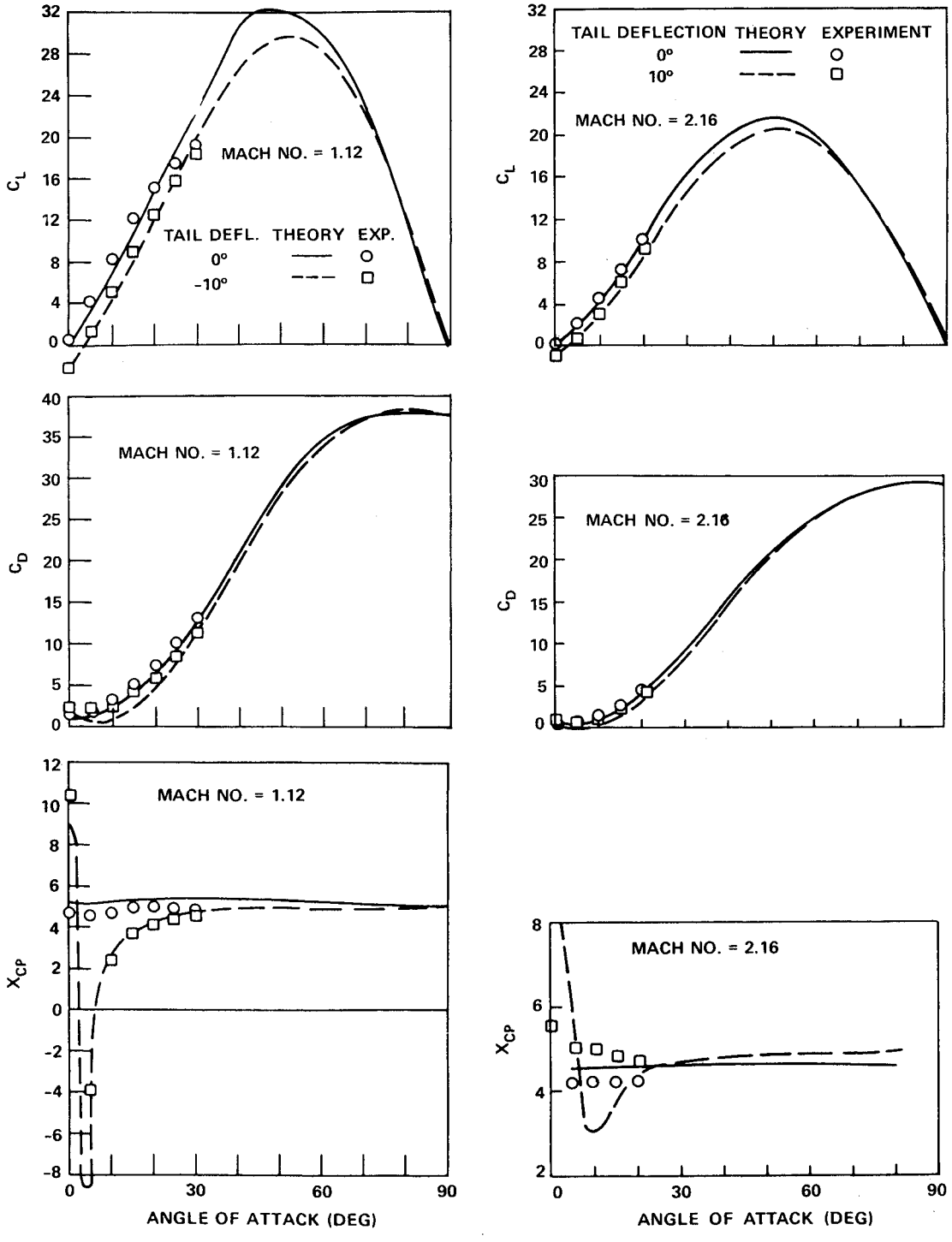

Fig. 6 Comparison of experimental data with theoretical results for configuration 2.

two-dimensional flat plate.[9] The equivalent flat plate area of the wing is taken as the projection of the wing area on the normal plane, $S_W \sin\alpha$.

The total drag increment for the tail surface is expressed as

$$\Delta C_{DT-\alpha} + \Delta C_{DT-\delta} = C_{DFP} \frac{S_T \sin(\alpha + \delta)}{S_{REF}} \qquad (22)$$

where $(\alpha + \delta)$ is the local tail angle of attack.

The total drag can be expressed as follows:

$$C_D = C_{D_0} + C_{D_i} \qquad (23)$$

where C_{D0} is the zero lift drag.

Pitching Moment Characteristics

The total pitching moment acting on the missile is the sum of the moments due to the lift and drag forces acting on the body, wings, and tails. Most methods for computing the pitching moment[1,5,8] consider only the moment due to lift. This is valid only for small angles of attack. If large angles of attack are to be considered, the moment must include the drag contribution. The body longitudinal pitching moment is determined directly, while the other components are determined only after the centers of pressure of the wing and tail surfaces are specified.

The body-alone pitching moment about X_{CG} is obtained

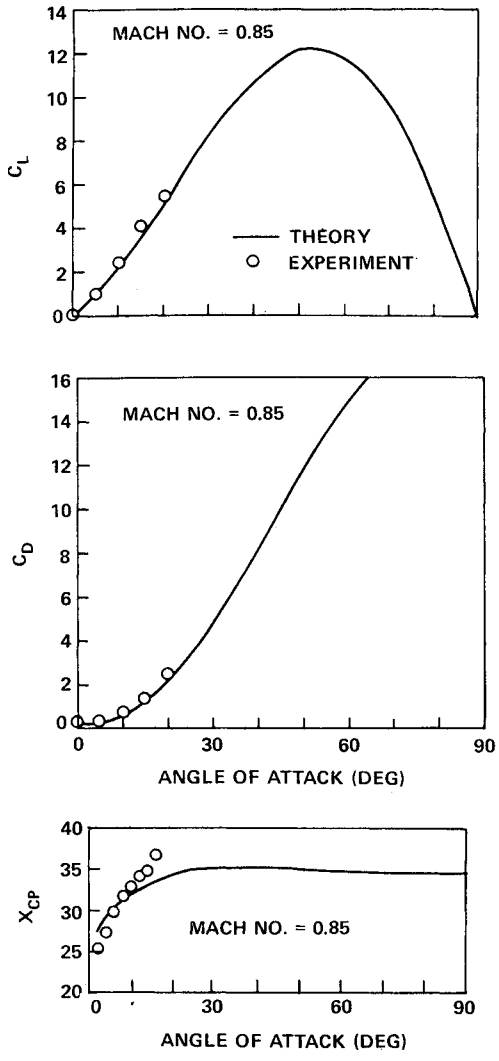

Fig. 7 Comparison of experimental data with theoretical results for configuration 3.

from Allen[2,3]: the expression is

$$C_{m_B} = (k_2 - k_1)\frac{V_B - S_B(l_B - X_{CG})}{S_{\text{REF}}\, l_{\text{REF}}} \sin 2\alpha \cos\alpha + \eta C_{d_c}\frac{S_P}{S_{\text{REF}}}\frac{X_{CG} - X_P}{l_{\text{REF}}}\sin^2\alpha \quad (24)$$

where $(k_2 - k_1)$, C_{d_c}, and η are given in Allen. This moment coefficient is based on an arbitrary reference length and area.

As noted above, the center-of-pressure locations for the wing and tail surfaces must be specified before their pitching moments can be determined. The linear lift of the aerodynamic surfaces is composed of two components: the lift on the surface in the presence of the missile body and the additional lift on the body due to the presence of a lifting surface. This means that in order to determine the linear pitching moment caused by the lifting surfaces, it is necessary to specify the center-of-pressure location for each of their linear components.

The center of pressure of the lift on the wing in the presence of the body as measured from the juncture of the wing leading edge and the body is obtained using curves given by Pitts et al. The reference point is transferred to the nose by the equation

$$C_{CPWB} = (X/C_r)_{WB}(C_r)_W + l_W \quad (25)$$

where $\bar{X}/C_r$ is obtained from Pitts et al.

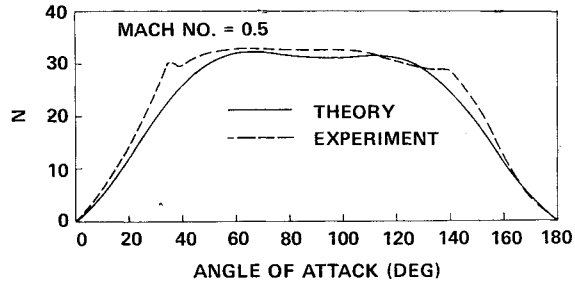

Fig. 8 Comparison of experimental data with theoretical results for configuration 4.

The center of pressure of the additional lift on the body in the presence of the wing is obtained using similar curves from Pitts et al. These curves are given for subsonic flow, and for supersonic flow with subsonic and supersonic leading edges, for various taper ratios. The center of pressure $\bar{X}_{BW}$, as obtained from these curves, is referred to the nose using Eq. (25).

The location of both centers of pressure for the tails, X_{CPTB} and X_{CPBT}, can also be obtained by the aforementioned procedure.

The centers of pressure for a given lifting surface are combined to obtain a single average center of pressure location for each set of aerodynamic surfaces. Care must be taken to include the effects of control surface deflections for the tail. The pitching moments can now be determined about the nose and transferred to X_{CG} using the equation

$$C_m = C_{m_B} + C_{m_W}(X_{CG} - X_{CPW})/X_{CPW} + C_{m_T}(X_{CG} - X_{CPT})/X_{CPT} \quad (26)$$

Results

The aerodynamic results are shown in Figs. 5–8 for four basic configuration types (Fig. 4). In general the results of this method agree well with experimental data. Unfortunately, a lack of experimental data to large α's (approaching 90°) limited meaningful comparisons. Although numerous other working comparisons have been made, only these are shown as representative of the configuration types and of the α ranges of interest. Most other experimental data are limited to α's approaching 15° or 20° as a maximum.

It is apparent from these comparisons that the stall characteristics are not adequately accounted for. This is not surprising since no specific attempt was made to predict stall. For very low aspect ratios, however, this is not serious, since the stall is nearly undetectable. This is borne out in the comparison of configuration 1 (Fig. 5). The apparent inadequacy of the stall prediction is demonstrated in the comparisons of configurations 2 and 3 (Figs. 6 and 8).

The comparisons of configuration 2 demonstrate the fin deflection capability of the method (Fig. 6). The lift and drag show good agreement at both Mach numbers with fins deflected and not deflected. The X_{CP} is predicted very well at $M = 1.12$, but at $M = 2.16$ the X_{CP} prediction with fins deflected deviates decidedly from the experimental curve. This deviation cannot be adequately explained. The drastic change in the experimental curves between $M = 1.12$ and $M = 2.16$ for fins deflected makes the accuracy of the experimental data questionable. Unfortunately, there are no intervening Mach numbers to establish a trend. Therefore, no conclusions can be drawn for this particular case without further supporting data.

The comparison of configuration 4 (Fig. 8) is the only available comparison to $\alpha = 180°$. Experimental axial force data were not sufficiently defined to warrant comparison, and center-of-pressure data were not compared because of the jet flap behind the base of the missile.[11] This drastically affects

X_{CP}, since this flap is shielded at low α's but its effects become more prominent as α grows. Since there is no provision to account for this in the prediction method, X_{CP} comparisons were not made.

References

[1] Pitts, W. C., Nielsen, J. N., and Kaattari, G. E., "Lift and Center of Pressure of Wing-Body-Tail Combinations at Subsonic, Transonic and Supersonic Speeds," Rept. 1307, 1957, NACA.

[2] Allen, H. J., "Estimation of the Forces and Moments Acting on Inclined Bodies of Revolution," RM A9126, March 1951, NACA.

[3] Allen, H. J. and Perkins, E. W., "Characteristics of Flow Over Inclined Bodies of Revolution," RM A50L07, March 1951, NACA.

[4] Flax, A. H. and Lawrence, H. P., "The Aerodynamics of Low-Aspect-Ratio Wings and Wing-Body Combinations," Rept. CAL-37, Sept. 1951, Cornell Aeronautical Lab., Buffalo, N. Y.; also *Proceedings of Third Anglo-American Aeronautical Conference*, Brighton, England, Sept. 1951, London, Royal Aeronautical Society, 1952.

[5] Eaton, P. T., "A Method for Predicting the Static Aerodynamic Characteristics of Low-Aspect-Ratio Configurations," Rept. 2216, June 1966, David Taylor Model Basin, Washington, D. C.

[6] Gersten, K., "Calculation of Non-Linear Aerodynamic Stability Derivatives of Aeroplanes," Rept. 342, 1961, 1962, Advisory Group for Aeronautical Research and Development, Paris.

[7] Franz, G. E., "Lift Curve Slopes of Low Aspect Ratio Wings at Transonic Speeds," Applied Mechanics TN AM-TN-2-63, June 1963, North American Aviation, Columbus, Ohio.

[8] Douglas Aircraft Co., "USAF Stability and Control DATCOM," Rev. W-P AFB, June 1969, Vol. 2, Wright-Patterson Air Force Base, Ohio.

[9] Hoerner, S. F., *Fluid Dynamic Drag*, 2nd ed., Sighard F. Hoerner, Midland Park, N. J., 1958.

[10] Dommasch, D. O., Sherby, S. S., and Connolly, T. F., *Airplane Aerodynamics*, Pitman, New York, 1961.

[11] Beil, W. J. et al., "Major Developments for the Jet Vane Controlled Bomber Defense Missile," BE-754-S-24, March 1955, Cornell Aeronautical Lab., Buffalo, N. Y.

MAY 1971 J. SPACECRAFT VOL. 8, NO. 5

Recent Work on Radio Frequency Ion Thrusters

HORST W. LOEB*
University of Giessen, West Germany

Based on demonstration of feasibility and on careful optimizations, the standardized 10-cm-diam radio frequency ion thruster RIT 10 of 100 ma, 1.1 kg, 309 w, and 71.5% thruster efficiency, equipped with power conditioning and control units, has reached laboratory prototype maturity. Two advanced concept definition studies are under way in preparation for space testing of an rf-engine-cluster by spiralling up a 350 kg-satellite, probably in 1976. Measurements on plasma diagnostics, ion extraction and focusing mechanism, beam distribution, etc. have been performed. Variation of ionizer's diameter from 4 to 20 cm, considering scaling laws and optimization of all the parameters, has been accomplished. A large vacuum test facility of 28 m³ volume is in operation.

Introduction

TEN years ago, there were two main types of electrostatic engines: the cesium contact drive and Kaufman's mercury bombardment thruster. However, the former type has the disadvantage that it cannot use mercury as the propellant, and the latter type suffered in the beginning from lifetime problems due to discharge cathode erosion. Therefore, we began at the Giessen University to examine,[1] optimize,[2] and prove the feasibility of use[3] of the rf ion source for electrostatic propulsion purposes. Basic plasma and beam diagnostic measurements have been undertaken. A new extraction and focusing mechanism has been applied. Lifetime runs and a 11,000 ignition test have been carried out.[4] Auxiliary components—vaporizer, isolator, fully transistorized rf-transmitter, plasma bridge neutralizer, power conditioning, and thruster control unit—have been developed. The standardized 10-cm-diam rf-engine is now being prepared by the industry for flight qualification. Besides RIT 10, a small 4-cm-diam thrust unit for attitude control and station-keeping, and 20-cm-diam engines for main propulsion missions are under optimization. In total, a team of 18 scientists is working on rf-electric propulsion at six test stands and two computers.

The rf-ion source works with an electrodeless, annular, self-sustaining discharge and produces a dense, nonisothermal, quasi-neutral mercury plasma. Some advantages in respect to the other ion engine types are: 1) with no dischange electrodes, lifetime problems are avoided; 2) because of an ion optical focusing effect, very high propellant efficiencies have been gained; 3) owing to the rf-discharge electrons' Maxwell distribution, only singly charged Hg^+ ions are observed, resulting in a beam homogeneity of 100%; 4) the rf-ion source is easy to assemble and control. From the beginning, the following objections arose: 1) It is more difficult to couple the discharge energy electrodelessly from the outside into the plasma than to display it inside by d.c. electrodes. 2) A spontaneous breakdown of the rf-discharge is possible only by increasing pressure or using a special igniter electrode. 3) To the usual electrostatic beam spreading a focusion aperture is added, causing a divergence efficiency drop of about 1%. 4) In the case of poor shielding some harmonics of the rf-transmitter could possibly disturb the

Presented as Paper 70-1102 at the AIAA 8th Electric Propulsion Conference, Stanford, Calif., August 31–September 2, 1970; submitted October 27, 1970; revision received December 30, 1970. This report is dedicated to W. Hanle on the occasion to his 70th birthday. The author thanks all his co-workers for assistance. This research is supported by the German Ministry of Education and Science (Contract RFF 3034).

* Professor, Head of Electric Propulsion Department, 1st Institute of Physics. Member AIAA.